Copyright © 2010 American Scientific Publishers
All rights reserved
Printed in the United States of America

Nanoscience and Nanotechnology Letters
Vol. 2, 308–314, 2010

Post-Buckling Deformation of Single-Walled Carbon Nanotubes

Qing Wei†, Meng Zheng†, and Changhong Ke*

Department of Mechanical Engineering, State University of New York at Binghamton, Binghamton, New York 13902, USA

We present a nanomechanical study of the post-buckling deformation of single-walled carbon nanotubes (SWNTs). One thin SWNT bundle is anchored as a clamped-hinged structure between a flexible atomic force microscopy (AFM) cantilever and a rigid manipulator probe by means of nanomanipulation inside a high resolution scanning electron microscope (SEM). Both the deformation curvatures of the clamped-hinged nanotube beam and the corresponding applied loads during the post-buckling deformation processes are concurrently measured, *in situ*, through recording the buckled nanotube beam shape and the deflection of the AFM cantilever, respectively, using the high resolution electron beam. Using our *in-situ* SEM nanomechanical testing platform, we perform tensile tests on the same nanotube structure to characterize its Young's modulus. Our experimental measurements of the post-buckling deformation curvatures of the bundled SWNTs and the corresponding applied loads are in reasonably good agreements with theoretical predictions based on a nonlinear elastica model. The results reported in this letter will be useful to the understanding of the structural deformation of one-dimensional nanostructures in the large displacement regime, and to the pursuit of their structural applications.

Delivered by Ingenta to:
State University of New York at Binghamton
IP : 128.226.14.2
Fri, 07 Jan 2011 17:31:37

Keywords: Carbon Nanotubes, Buckling, Young's Modulus, Scanning Electron Microscopy.

Carbon nanotubes[1] (CNTs) are one of the most exciting one-dimensional (1D) nanostructures that emerged during the past two decades, and have received tremendous attention from the research community. CNTs are found to possess extraordinary mechanical, electrical, and chemical properties,[2–6] and are promising for a number of applications, such as composites, electronics, sensors and biomedicines.[7–11] Studies have shown that CNTs possess excellent elastic behaviors even in the large displacement, tension and rotation regimes.[12–14] Due to their high-aspect-ratio characteristics, CNTs may easily buckle under very tiny compressive loads. Therefore, understanding the buckling behavior of CNTs is important to many of their structural applications. Because the critical buckling load for a slender beam is linearly proportional to its Young's modulus, mechanical buckling of CNTs has been employed to estimate the nanotube's Young's modulus by using both experimental and theoretical techniques.[15–20] The present work is partially inspired by the recent study reported by Mikita on the theoretical analysis of the post-buckling deformation of a clamped-hinged carbon nanotube.[20] In that work, the author treated the nanotube as an inextensible elastica and derived closed-form solutions on its post-buckling deformation. To the best of our knowledge, no reported experimental study about the post-buckling deformation of free-standing clamped-hinged carbon nanotubes is yet available. That is, in part, due to the technical challenges associated with the precise manipulation of nanostructures and the concurrent measurements of the mechanical response of the nanostructure and the corresponding applied load with adequate resolutions.[21] In this work, we quantitatively investigate the post-buckling deformation of free-standing single-walled carbon nanotubes using *in-situ* scanning electron microscopy (SEM) nanomechanical characterization techniques, which enable the high resolution concurrent measurements of both the deformation of the buckled nanotube and the applied load. Our experimental results are interpreted using the nonlinear elastica model reported in Ref. [20].

The configuration of a buckled clamped-hinged nanotube beam, denoted as ABC, is schematically shown in Figure 1(a). A horizontal compressive force P is applied to the hinged end C to initiate the buckling of the nanotube. The resultant vertical reaction force at the hinged end is denoted as R. The slope angle of the beam at the hinged end is denoted as θ_0. Our *in-situ* scanning electron microscopy

*Author to whom correspondence should be addressed.
†These two authors contributed equally to this work.

 1941-4900/2010/2/308/007 doi:10.1166/nnl.2010.1099

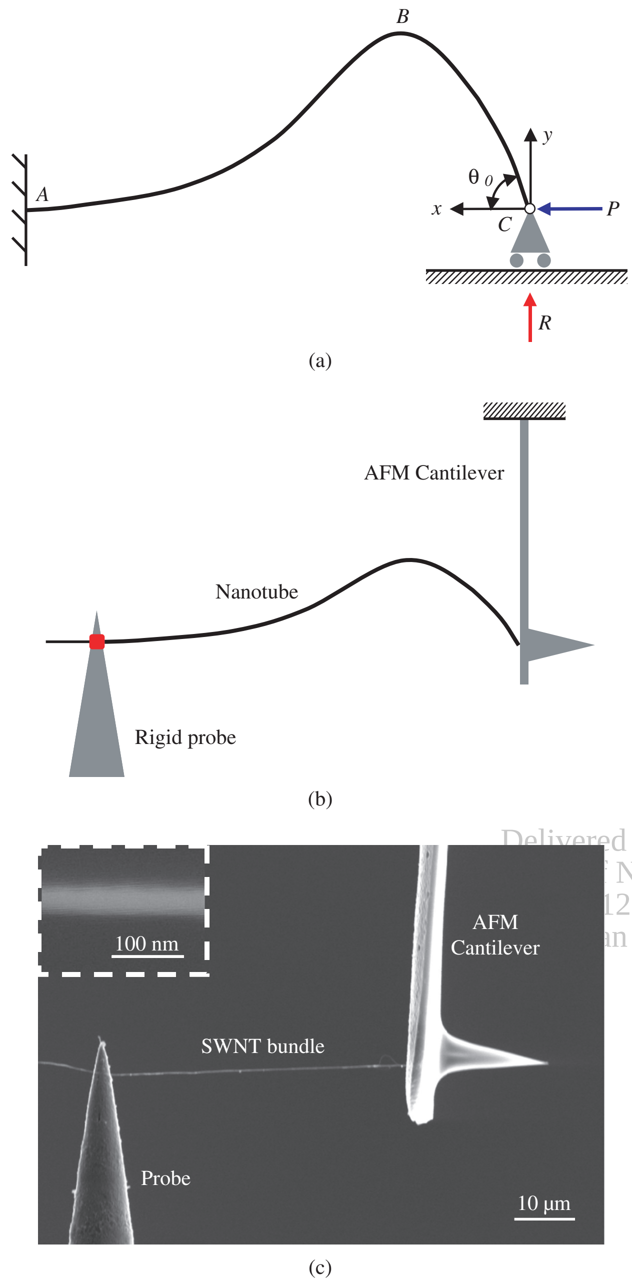

Fig. 1. (a) Schematic of the post-buckling deformation of a clamped-hinged slender beam in the Cartesian coordinate system; (b) schematic of our *in-situ* SEM nanomechanical characterization scheme; (c) SEM image of one of our tested thin single-walled carbon nanotube bundles. The inset shows a high magnification view of the nanotube structure.

nanomechanical characterization scheme is illustrated in Figure 1(b). In this testing scheme, one nanotube beam is placed horizontal and clamped-hinged between one movable rigid tungsten manipulator probe and one fixed flexible atomic force microscopy (AFM) cantilever. The manipulator probe is attached to a 3D piezo-stage with the closed-loop feedback control, which possesses motion resolution of 1 nm in the XYZ directions.[22,23] This probe is controlled to move closer to the AFM cantilever at a speed of ~1 μm/s and a step size in the range of 0.01~2 μm, thus exerting a compressive force on the nanotube beam and resulting in a deflection of the vertically placed AFM cantilever. Both the buckling deformation of the nanotube and the deflection of the AFM cantilever stay in the horizontal plane and are perpendicular to the high resolution electron beam. Therefore, both the deformation curvature of the buckled nanotube and the applied load can be experimentally quantified by digitally analyzing the recorded high resolution SEM images of the nanotube and the AFM cantilever. Figure 1(c) shows one of our nanotube beams held between a manipulator probe and an AFM cantilever. The nanotube beam is a thin single-walled carbon nanotube (SWNT) bundle, which was originally synthesized using chemical vapor deposition (CVD) methods and then obtained using a simple mechanical scratch approach.[13,17] Our prior transmission electron microscopy (TEM) studies have confirmed that the tubes in the bundle obtained using the mechanical scratch approach are parallel and held tightly to one another, presumably by van der Waals interactions.[13,17] The length and lateral width of this nanotube beam are measured to be 21.06 μm and 45 nm (see the inset in Fig. 1(c)), respectively. The attachment of the nanotube beam to the probe was enhanced by using the electron beam induced deposition (EBID) of hydrocarbon molecules available in the electron microscope chamber,[22,24,25] and is considered as a clamped connection. This boundary constraint is consistent with our later experimental observation that no displacement or rotation occurred at the attachment point during the whole nanomechanical testing process. The contact between the nanotube and the backside surface of the AFM cantilever was by van der Waals interactions only, and is considered as a joint or hinged connection. The joint boundary constraint indicates that the end portion of nanotube beam in contact with the AFM cantilever surface can only rotate with respective to the contact point during the buckling process, while no displacement or sliding occurs. This boundary condition is also consistent with our experimental observations.

Figures 2(a) and (b) show two selected SEM snapshots of the post-buckling deformation of the nanotube beam shown in Figure 1(c). It can be clearly seen that the deformation curvature of the buckled nanotube at each testing step can be visualized and quantitatively measured from the captured SEM images. Figures 2(d) and (e) show two selected SEM snapshots of the post-buckling deformation of the same nanotube beam as shown in Figures 2(a–b) whereas the AFM cantilever was flipped-over and the right end of the nanotube beam was attached to the tip of the AFM probe by the van der Waals interactions. For the SEM snapshots shown in Figure 2, the original image resolution is 25 nm per pixel. We increase our image measurement resolutions by one order of magnitude to 2.5 nm by analyzing the recorded high resolution SEM images using the two dimensional (2D)

Delivered by Ingenta to:
f New York at Binghamton
128.226.14.2
an 2011 17:31:37

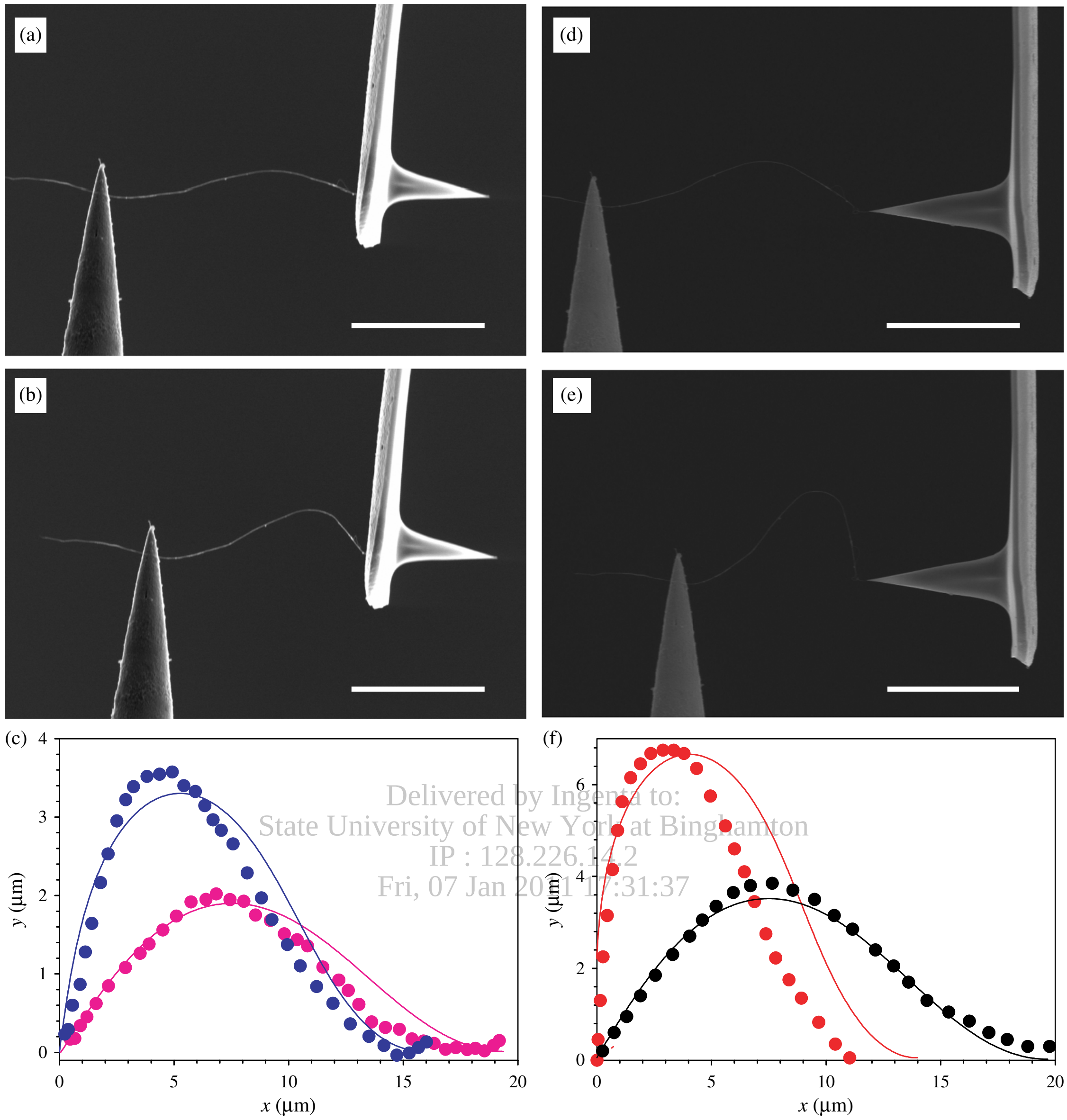

Delivered by Ingenta to:
State University of New York at Binghamton
IP : 128.226.14.2
Fri, 07 Jan 2011 17:31:37

Fig. 2. (a, b) Selected SEM snapshots of the post-buckling deformation of the SWNT bundle shown in Figure 1(c). The right end of the nanotube structure was attached to the backside of the AFM cantilever; (c) the comparison between experimental measurements and theoretical predictions on the post-buckling deformation curvatures of the SWNT bundles shown in (a) and (b); (d, e) selected SEM snapshots of the buckling deformation of the same SWNT bundle shown in Figures 2(a) and (b). The right end of the nanotube structure was attached to the tip of the AFM cantilever; (f) the comparison between experimental measurements and theoretical predictions on the post-buckling deformation curvatures of the SWNT bundles shown in (d) and (e). The scale bars represents 10 μm.

digital image correlation (DIC) technique.[26] In brief, DIC is a well-accepted metrology technique for micro- and nanoscale displacement/deformation measurements.[27] By numerically processing the captured digital images of a test object before and after deformation through calculating the motion of the image points based on the gray intensities of neighboring pixels, DIC is capable of directly providing displacement/deformation at a sub-pixel accuracy. In our measurements, we employed two types of Si AFM cantilevers from K-TEK Nanotechnology with nominal spring constants of 0.03 N/m and 0.1 N/m, respectively. The spring constant of each of our employed AFM cantilevers was carefully calibrated using a thermal tuning method based on the energy equipartion theorem.[28, 29] The calibrated spring constant for the AFM cantilever showed in Figures 2(a and b) is 0.064 N/m, while 0.103 N/m for the one shown in Figures 2(d and e). Assuming that the deflection measurement sensitivity using DIC techniques is one-half of its pixel resolution (i.e., 1/20 of a pixel), the force measurement sensitivity for the experiments shown in Figures 2(a and b) is calculated to be 0.08 nN, while 0.129 nN for the experiments shown in Figures 2(d and e). Our *in-situ* experiments also reveal that the buckled nanotube beam exhibits purely elastic behavior and no permanent plastic deformation is observed.

We employ a nonlinear elastica model to theoretically predict the post-buckling deformation of the nanotube beam and to interpret our experimental measurements. The clamped-hinged CNT beam is considered as an inextensible elastica rod and the governing equation of its deformation is given by[20]

$$EI\frac{\mathrm{d}^2\theta}{\mathrm{d}s^2}+P\sin\theta-R\cos\theta=0 \quad (1)$$

where s is the arc length along the beam measured from the hinged end, θ is the angle between the tangent of the beam at s and the x-axis; E and I are the Young's modulus and the moment of inertia of the nanotube beam, respectively; R is the vertical reaction force at the hinged end and is given by $R=P\tan\alpha$, in which α is the angle between P and R. The deformation curvature of the buckled nanotube beam in the Cartesian coordinate system can be obtained by considering $\mathrm{d}x=\mathrm{d}s\cdot\cos\theta$ and $\mathrm{d}y=\mathrm{d}s\cdot\sin\theta$. The boundary conditions of the clamped-hinged nanotube beam are $(\mathrm{d}\theta/\mathrm{d}s)(0)=0$, $\theta(l)=0$, $x(0)=0$, $y(0)=0$, and $y(l)=0$. The closed-form solution of Eq. (1) was previously reported by Mikita,[20] which is briefly summarized here.

Delivered by Ingenta to:
State University of New York at Binghamton
IP : 128.226.1.42
Fri, 07 Jan 2011 17:31:57

Letting $k=\sin((\theta_0-\alpha)/2)$ and $n=\sin(\alpha/2)/k$, Eq. (1) can be transformed into[20]

$$\frac{n\sqrt{1-k^2n^2}}{1-2k^2n^2}\left[3(2E(k)-K(k))+\int_0^{\sin^{-1}n}\frac{2k^2\sin^2 t-1}{\sqrt{1-k^2\sin^2 t}}\,dt\right]-\sqrt{1-n^2}=0 \quad (2)$$

where $K(k)$ and $E(k)$ are the complete elliptic integrals of the first and second kinds, respectively. By numerically solving Eq. (2), the relationship between variables n and k can be obtained. Then, α and θ_0 can be obtained as a function of k by considering $\alpha=2\sin^{-1}(nk)$ and $\theta_0=\alpha+2\sin^{-1}k$, respectively. The compressive force P is given by $P=(EI\beta^2)/l^2$, in which $\beta=\sqrt{1-2k^2n^2}[3K(k)-\int_0^{\sin^{-1}n}dt/(\sqrt{1-k^2\sin^2 t})]$. Therefore, the respective dependences of α, θ_0, and R on P can be obtained. The detailed formulation for the deformation curvature of the buckled beam in the Cartesian coordinate system, i.e., $x(s)$ and $y(s)$, is also given in Ref. [20].

By using the above model, we theoretically predict the post-buckling deformation of the nanotube beam shown in Figure 1(c), and compare theoretical predictions with the experimental measurements shown in Figure 2. Figure 2(c) shows the comparison between experimental measurements (dotted curves) and theoretical predictions (solid curves) for the SEM snapshots shown in Figures 2(a and b). Similarly, Figure 2(f) shows the comparison between experimental measurements and theoretical predictions for the SEM snapshots shown in Figures 2(d and e). From the comparison curves shown in Figures 2(c and f), we can conclude that the experimental measurements and theoretical predictions on the post-buckling deformation curvatures of the nanotube beam are in reasonably good agreements, except for the measurement shown in Figure 2(e). From Figure 2(e), we notice that the portion of the nanotube close to the contact with the AFM tip experiences substantial bending deformation. Therefore, the contact between the nanotube and the AFM tip may not be simply recognized as a hinged connection. On the other hand, the black curves in Figure 2(f) exhibit good agreement between experimental measurements and theoretical predictions for the measurement shown in Figure 2(d). This observation suggests that the attachment of the nanotube to the AFM tip can be reasonably simplified as a hinged connection when the post-buckling of the nanotube is in its early stage. Nonetheless, our results suggest that boundary conditions may significantly affect the post-buckling deformation curvature of the nanotube beam. It is noted that the theoretically predicted post-buckling deformation curvatures as shown in Figures 2(c and f) are independent of the elastic rigidity of the nanotube beam EI. In order to theoretically predict the compressive force P that was exerted on the buckled nanotube, we need to first quantify the Young's modulus and the moment of inertia of the tested nanotube beam.

By employing the *in-situ* SEM nanomechanical testing scheme as illustrated in Figure 1(b), we performed tensile tests[24] on the same nanotube beam as employed in the buckling tests. The attachments of the nanotube to both the manipulator probe and the AFM tip were strengthened using EBID of hydro-carbon molecules. For the tensile test, the manipulator probe was controlled to move away from the AFM cantilever, thus exerting a tensile force on the nanotube beam as well as the AFM cantilever. The deformation of the nanotube and the deflection of the AFM cantilever at each tensile test step were first captured by using the high resolution electron beam, and then quantified by analyzing the recorded SEM images using the DIC technique. Selected SEM snapshots of the tensile testing of the nanotube beam are shown in Figures 3(a–c). Figure 3(a) shows the starting stage of the tensile test where the nanotube was aligned as a straight rod. Figure 3(b) shows that the nanotube was under significant tension, which can be inferred from the prominent deflection of the AFM cantilever compared with Figure 3(a). Figure 3(c) shows that the nanotube was detached from the AFM probe and the deflection of the AFM cantilever was fully recovered, indicating the ending of the tensile test.

We assume a solid circular cross-section for the nanotube bundle, meaning that the diameter of the bundle is

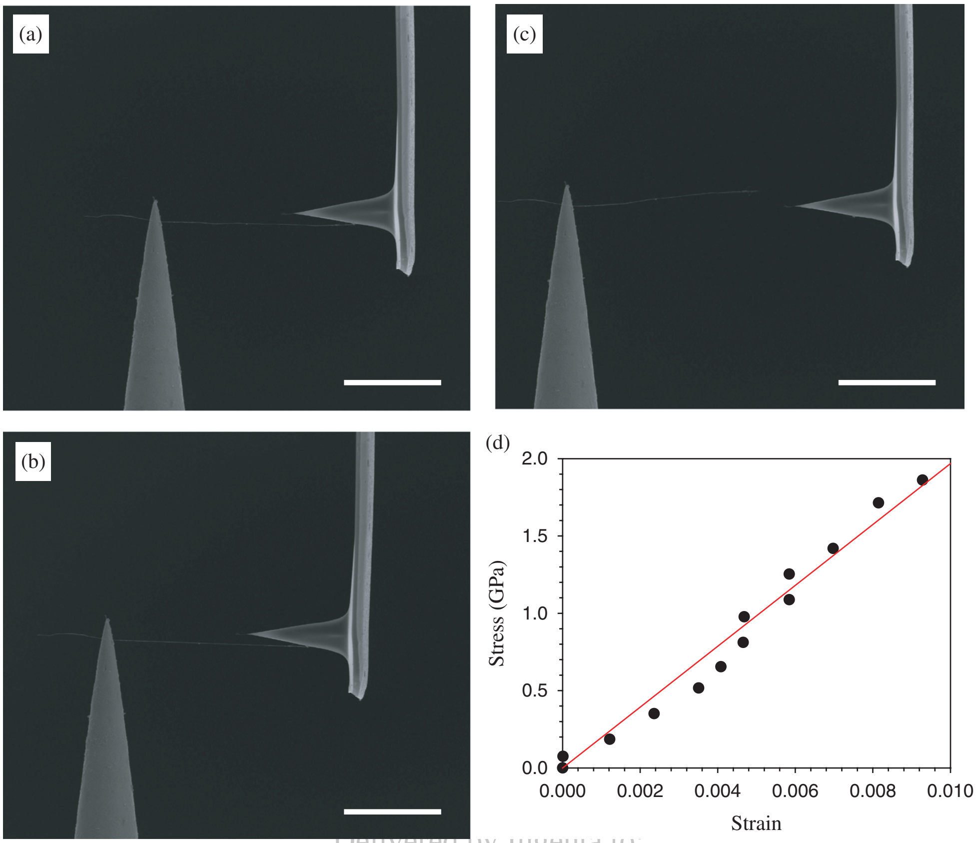

Delivered by Ingenta to:
State University of New York at Binghamton
IP : 128.226.14.2
Fri, 07 Jan 2011 17:31:37

Fig. 3. (a–c) Selected SEM snapshots of *in-situ* SEM tensile testing of the SWNT bundle shown in Figure 1(c). (d) The calculated stress–strain curve for the tested SWNT bundle. The scale bars represents 10 μm.

identical to its lateral width, 45 nm. The calculated tensile stress–strain relationship of the tested nanotube bundle based on our *in-situ* tensile measurements is shown in Figure 3(d). It is clear that the tensile stress and strain shows a nearly linear relationship. The Young's modulus of the nanotube bundle, which was measured as the slope of the stress–strain curve, is found to be 196.75 GPa. It is noted that the measured Young's modulus of the nanotube bundle is significantly lower than that of individual SWNTs ($\sim$1 TPa).[6] This observed discrepancy in Young's modulus of nanotubes is likely due to the fact that the inter-tube van der Waals interaction in bundled nanotubes is significantly weaker than the axial strength of individual tubes that is ascribed to the covalent C–C bonding.[17,30] We want to highlight that the measured Young's modulus of the bundled SWNTs by using the tensile test approach is consistent with our previously reported values (140$\sim$212 GPa) based on the tube–tube interfacial binding interaction in an adhesion-driven buckled nanotube configuration. The bundled nanotubes tested in both studies are from the same batch of sample.[17]

The bending rigidity of the tested nanotube bundle shown in Figure 1(c) is calculated to be $EI = 3.96 \times 10^{-20}$ N $\cdot$ m. For clamped-hinged columns, the critical buckling load is given by $P_{cr} = (2.05\pi^2/L^2)EI$. For our tested nanotube beam, the critical buckling force is calculated to be $P_{cr} = 1.81$ nN. For the buckled nanotube beam shown in Figure 2(d), the measured applied load through quantifying the deflection of the AFM cantilever is 1.81 nN, which is slightly lower than the theoretically predicted value, 1.85 nN. For the measurements shown in Figures 2(a and b), due to the fact that the initial position of the AFM cantilever was not recorded, we are not able to experimentally quantify the respective applied loads. Nonetheless, we are able to quantify the load difference between these two measurements from the captured high resolution SEM images, which is 0.15 nN. The corresponding theoretical prediction is 0.13 nN. Considering the force measurement sensitivity of our *in-situ* nanomechanical testing scheme, we can see that the experimental measurements and the theoretical predictions on the applied load are in reasonably good agreements. The variation of the nanotube beam cross-section along its length and defects in the nanotube beam are two possible sources accounting for the observed deviations between experimental measurements and theoretical predictions. The good agreements between the experimental measurements and theoretical predictions on both the post-buckling deformation curvature and the applied load strongly suggest that the deformation behavior of carbon nanotubes in the large displacement regime can be reasonably predicted by using the nonlinear continuum elastica theory. The vertical reaction force at the hinged end, R, is not directly measurable in our *in-situ* mechanical testing system. The theoretically predicted values for R for the measurements shown in Figures 2(a), (b), (d) are 0.29 nN, 0.68 nN, and 0.29 nN, respectively. Since the vertical force R is only a fraction of the horizontal force P and is in the sub-nN regime, a force detecting system with measurement sensitivity in the order of 10^{-2} nN or better is technically demanded for accurate measurements.

By using the nonlinear elastica model, we conduct a detailed investigation of the post-buckling deformation of the clamped-hinged nanotube beam shown in Figure 1(c) under the compressive load and our results are presented in Figure 4. The four curves in Figure 4(a) reveal the evolution of the post-buckling deformation curvature of the nanotube beam under different compressive loads. It can be seen that two deformation curves (i.e., the black and blue curves) correspond to $P = 1.9$ nN, indicating that a bifurcation occurs in the post-buckling deformation of

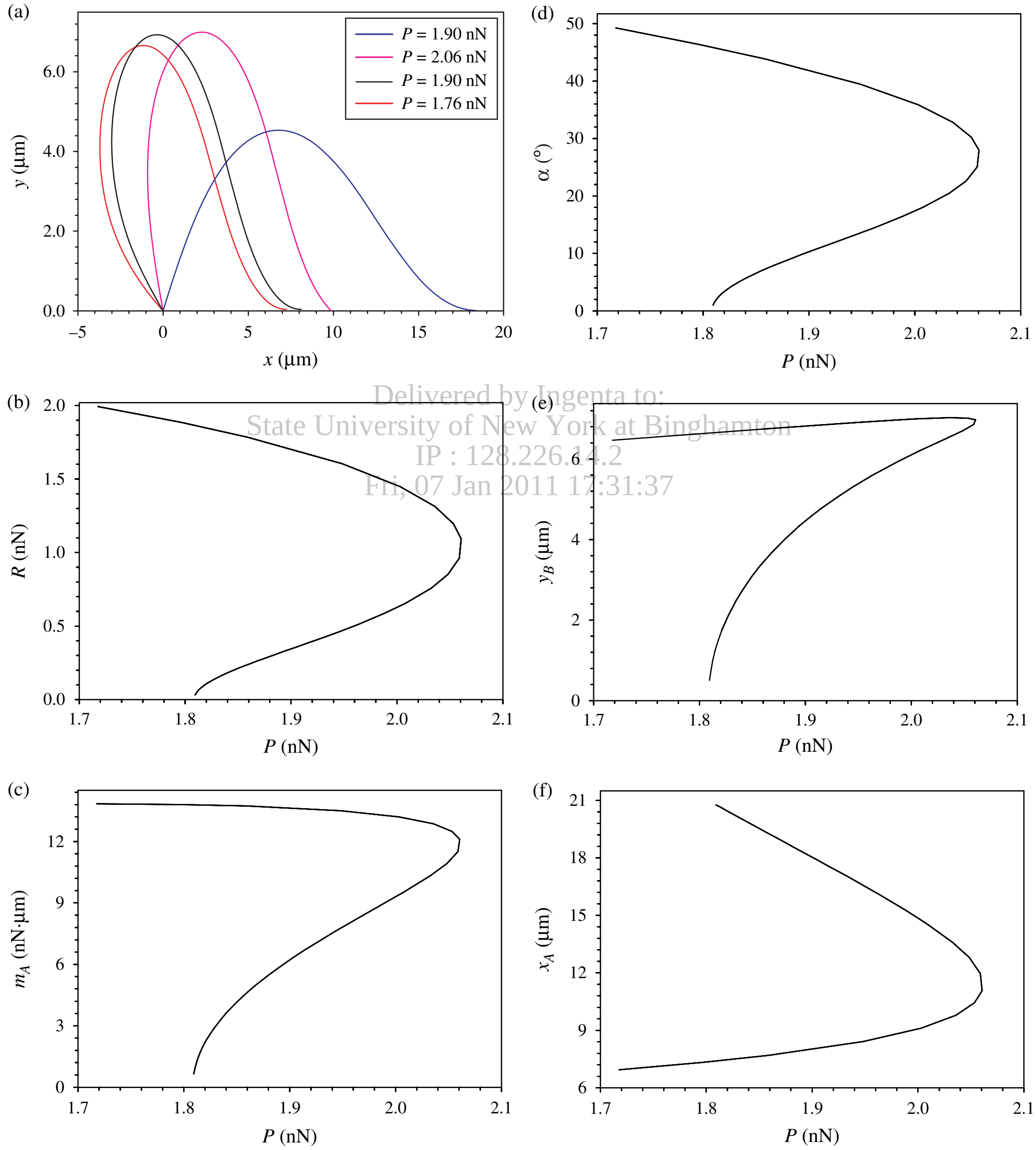

Delivered by Ingenta to:
State University of New York at Binghamton
IP : 128.226.44.2
Fri, 07 Jan 2011 17:31:37

Fig. 4. The dependences of selected parameters of the theoretically predicted post-buckling deformation of the nanotube beam shown in Figure 1(c) on the compressive force P: (a) the post-buckling deformation curvature of the nanotube beam; (b) R, the vertical reaction force at the hinged end; (c) m_A, the reaction moment at the clamped end A; (d) α, the angle between the horizontal force P and vertical force R at the hinged end; (e) y_B, the height of the buckled nanotube; (f) x_A, the horizontal span of the buckled nanotube.

the clamped-hinged nanotube beam. Similar bifurcation phenomenon is also exhibited in the characteristic curves shown in Figures 4(b–f), which illustrate the respective dependences of the following parameters on the applied load P: the vertical reaction force at the hinged end, R; the reaction moment at the clamped end A, m_A; the angle between the horizontal force P and vertical force R at the hinged end, α; the height of the buckled nanotube, y_B; the horizontal span of the buckled nanotube, x_A. The maximum applied load P is calculated to be 2.06 nN. The bifurcation shown in Figure 4 suggests that the applied load on the post-buckled structure is strongly modulated by its elastic deformation, which is clearly in the large displacement regime.

In this letter, the post-buckling deformation of a thin SWNT bundle is investigated using a combined experimental-theoretical approach. The elastic deformation of the post-buckled nanotube beam is experimentally characterized using an *in-situ* electron microscopy nanomechanical testing scheme, and theoretically predicted using a nonlinear elastica model. The experimental measurements on both the post-buckling deformation curvature of the nanotube beam and the applied load are in reasonably good agreements with the theoretical predictions. The results reported in this paper will be useful to the understanding of the structural deformation of one-dimensional nanostructures in the large displacement regime, and to the pursuit of their structural applications.

This work was supported by the State University of New York at Binghamton. Acknowledgment is made to the Donors of the American Chemical Society Petroleum Research Fund for partial support of this research. The *in-situ* scanning electron microscopy measurements were performed using the facilities in the Analytical and Diagnostics Laboratory at Binghamton University's Small Scale Systems Integration and Packaging Center (S^3IP).

Delivered by Ingenta to: State University of New York at Binghamton IP : 128.226.1... Fri, 07 Jan 2011 17:31:37

References and Notes

1. S. Iijima, *Nature* 354, 56 **(1991)**.
2. D. Qian, G. J. Wagner, W. K. Liu, M. F. Yu, and R. S. Ruoff, *Applied Mechanics Review* 55, 495 **(2002)**.
3. P. L. McEuen, M. S. Fuhrer, and H. K. Park, *IEEE Transactions on Nanotechnology* 1, 78 **(2002)**.
4. T. Kuzumaki and Y. Mitsuda, *Appl. Phys. Lett.* 85, 1250 **(2004)**.
5. B. Liu, H. Jiang, H. T. Johnson, and Y. Huang, *Journal of the Mechanics and Physics of Solids* 52, 1 **(2004)**.
6. M. S. Dresselhaus, G. Dresselaus, and P. Avouris, Carbon Nanotubes, Springer, Berlin **(2001)**.
7. H. G. Craighead, *Science* 290, 1532 **(2000)**.
8. B. Mahar, C. Laslau, R. Yip, and Y. Sun, *IEEE Sens. J.* 7, 266 **(2007)**.
9. J. N. Coleman, U. Khan, and Y. K. Gun'ko, *Adv. Mater.* 18, 689 **(2006)**.
10. Z. Liu, S. Tabakman, K. Welsher, and H. J. Dai, *Nano Res.* 2, 85 **(2009)**.
11. C. H. Ke and H. D. Espinosa, *Appl. Phys. Lett.* 85, 681 **(2004)**.
12. M. R. Falvo, G. J. Clary, R. M. Taylor, V. Chi, F. P. Brooks, S. Washburn, and R. Superfine, *Nature* 389, 582 **(1997)**.
13. C. Ke, M. Zheng, G. Zhou, W. Cui, N. Pugno, and R. N. Miles, *Small* 6, 438 **(2010)**.
14. M. Zheng and C. Ke, *Small* 6, 1647 **(2010)**.
15. D. Y. Khang, J. L. Xiao, C. Kocabas, S. MacLaren, T. Banks, H. Q. Jiang, Y. Y. G. Huang, and J. A. Rogers, *Nano Lett.* 8, 124 **(2008)**.
16. J. Xiao, H. Jiang, D. Y. Khang, J. Wu, Y. Huang, and J. A. Rogers, *J. Appl. Phys.* 104, 033543 **(2008)**.
17. C.-H. Ke, M. Zheng, and I.-T. B. G.-W. Zhou, *J. Appl. Phys.* 107, 104305 **(2010)**.
18. L. Liu, M. H. Zhao, Q. L. Zhou, and X. Chen, *Mechanics Research Communications* 35, 256 **(2008)**.
19. H. J. Qi, K. B. K. Teo, K. K. S. Lau, M. C. Boyce, W. I. Milne, J. Robertson, and K. K. Gleason, *Journal of the Mechanics and Physics of Solids* 51, 2213 **(2003)**.
20. Y. Mikata, *Acta Mechanica* 190, 133 **(2007)**.
21. Y. Zhu, C. Ke, and H. D. Espinosa, *Experimental Mechanics* 47, 7 **(2007)**.
22. C. H. Ke and H. D. Espinosa, *Small* 2, 1484 **(2006)**.
23. C. H. Ke, N. Pugno, B. Peng, and H. D. Espinosa, *Journal of the Mechanics and Physics of Solids* 53, 1314 **(2005)**.
24. M. F. Yu, O. Lourie, M. J. Dyer, K. Moloni, T. F. Kelly, and R. S. Ruoff, *Science* 287, 637 **(2000)**.
25. W. Ding, D. A. Dikin, X. Chen, R. D. Piner, R. S. Ruoff, E. Zussman, X. Wang, and X. Li, *J. Appl. Phys.* 98, 014905 **(2005)**.
26. The image analysis using digital image correlation (DIC) techniques is implemented using the DIC software from http://opticist.org/.
27. B. Pan, K. M. Qian, H. M. Xie, and A. Asundi, *Measurement Science and Technology* 20, 062001 **(2009)**.
28. E. L. Florin, M. Rief, H. Lehmann, M. Ludwig, C. Dornmair, V. T. Moy, and H. E. Gaub, *Biosens. Bioelectron.* 10, 895 **(1995)**.
29. C. Ke, M. Humeniuk, H. S.-Gracz, and P. E. Marszalek, *Phys. Rev. Lett.* 99, 018302 **(2007)**.
30. J. P. Lu, *Phys. Rev. Lett.* 79, 1297 **(1997)**.

Received: 10 August 2010. Accepted: 24 September 2010.